Impact of the Estimation of Synchronous Machine Rotor Speeds on Wide-Area Damping Controllers

Georgios Tzounas, *Student Member, IEEE*, Federico Milano, *Fellow, IEEE*
School of Electrical and Electronic Engineering, University College Dublin, Ireland
georgios.tzounas@ucdconnect.ie, federico.milano@ucd.ie

***Abstract*—The paper focuses on the ability of decentralized wide area power system stabilizers to damp inter-area oscillations when fed with rotor speed estimations of remote synchronous machines. Rotor speeds are estimated by means of the Frequency Divider Formula (FDF), which has been recently proposed on the IEEE Transactions on Power Systems by the second author. Different remote signals, namely rotor speeds and the frequency of the Center of Inertia (COI) are compared with bus frequency estimations using the well-known two-area test system. The impact of realistic communication delays on the damping of the oscillations is also discussed.**

***Index Terms*—Inter-area oscillations, wide area signals, frequency divider formula, phase-locked loop, time delays, modal analysis, transient stability.**

I. Introduction

A. Motivation

The control of electric energy systems involves the solution of several practical issues, especially when measurement signals need to be transmitted over different areas. These issues include the choice of a proper control strategy, the selection of actuators and remote feedback signals, and the assessment of the impact of time delays, e.g., through modal analysis. This work focuses on the estimation and utilization of remote signals such as rotor speeds of synchronous machines and the frequency of the Center of Inertia (COI) for the purpose of wide area damping control.

B. Literature Review

Inter-area oscillations occur in interconnected power systems when a group of coherent synchronous machines in one area oscillates with respect to a group in another area. The natural frequency of such oscillations is typically in the range of 0.1-1 Hz [1]. Inter-area modes are associated with the dynamics of power transfers [2] and hence, their importance has grown in recent years due to increasing power exchanges among national grids.

The conventional approach of installing a Power System Stabilizer (PSS) with local measurements is not adequate for damping inter-area modes [3]. Remote signals with high observability have been proven to be effective to damp such oscillations [2], [4]. These signals can be obtained through measurement units and transmitted to the Wide Area Damping Controller (WADC) through a communication network [5]. The mediation of the communication network in remote signal transmission introduces stochastic and quasi-periodic delays [6], [7].

A critical aspect of WADCs is the selection of the most effective stabilizing signals. The geometric observability/controllability method is a simple approach that allows determining the signals with maximum robustness and best performance [8]. Regarding frequency-based wide area signals, the differential rotor speed of two synchronous machines from different areas is widely utilized in literature. For example, relevant references are [4], [9]. Other signals that have been proposed are the frequency at synchronous machine terminal buses [10], and the frequency of the COI of a remote area [11].

While rotor speed signals can be easily obtained in simulations, only bus frequency estimations are available in practice, e.g., through the Phase-Locked Loop (PLL) devices of phasor measurement units (PMUs). To overcome this issue, we use the recently proposed Frequency Divider Formula (FDF) [12] to estimate generator rotor speeds [13] as well as the frequency of the COI [14] based on PMU measurements.

C. Contributions

The paper provides a thorough comparison of the effectiveness of different frequency signals on the dynamic response of a Wide Area Power System Stabilizer (WAPSS). These signals are synchronous machine rotor speeds, bus frequencies and COI frequency. All signals are properly modelled using realistic PMU measurements and estimated through the FDF. Moreover, a variety of PLL implementations are compared to define the most suitable model for WAPSS applications. Finally, a discussion on the impact of realistic time-varying delays on the dynamic response of WAPSS is provided.

D. Organization

The remainder of the paper is organized as follows. Section II recalls the power system state space model and presents the applied control scheme. Section II also outlines the delay model utilized in this work. Section III outlines the concept of the FDF for wide area signals frequency estimation. Section IV discusses the case study by carrying small-signal and transient stability analyses on the two-area test system. Conclusions are drawn and future work is outlined in Section V.

This work was supported by: Science Foundation Ireland, by funding Georgios Tzounas and Federico Milano under Grant No. SFI/15/IA/3074.

II. Power System Model and Control Scheme

A. State Space Representation

Power system dynamics are conveniently described through a set of Differential Algebraic Equations (DAEs):

$$\begin{aligned} \dot{\boldsymbol{x}} &= \boldsymbol{f}(\boldsymbol{x}, \boldsymbol{y}, \boldsymbol{u}) \\ \boldsymbol{0} &= \boldsymbol{g}(\boldsymbol{x}, \boldsymbol{y}, \boldsymbol{u}) \ , \end{aligned} \tag{1}$$

where $\boldsymbol{f}$ ($\boldsymbol{f} : \mathbb{R}^{n+m+p} \rightarrow R^n$), $\boldsymbol{g}$ ($\boldsymbol{g} : \mathbb{R}^{n+m+p} \rightarrow R^m$) are the differential and algebraic equations; $\boldsymbol{x}$, $\boldsymbol{x} \in \mathbb{R}^n$, and $\boldsymbol{y}$, $\boldsymbol{y} \in \mathbb{R}^m$, are the state and algebraic variables, respectively; and $\boldsymbol{u}$, $\boldsymbol{u} \in \mathbb{R}^p$, are the controlled inputs. Differentiating (1) around an equilibrium point $(\boldsymbol{x}_0, \boldsymbol{y}_0, \boldsymbol{u}_0)$ and eliminating the algebraic variables leads to the following Multiple-Input Multiple-Output (MIMO) state space model:

$$\begin{aligned} \Delta\dot{\boldsymbol{x}} &= \boldsymbol{A}\Delta\boldsymbol{x} + \boldsymbol{B}\Delta\boldsymbol{u} \\ \Delta\boldsymbol{w} &= \boldsymbol{C}\Delta\boldsymbol{x} + \boldsymbol{D}\Delta\boldsymbol{u} \ , \end{aligned} \tag{2}$$

where $\boldsymbol{A} = \boldsymbol{f_x} - \boldsymbol{f_y}\boldsymbol{g_y}^{-1}\boldsymbol{g_x}$, $\boldsymbol{B} = \boldsymbol{f_u} - \boldsymbol{f_y}\boldsymbol{g_y}^{-1}\boldsymbol{g_u}$; $\boldsymbol{f_x}$, $\boldsymbol{f_y}$, $\boldsymbol{f_u}$, $\boldsymbol{g_x}$, $\boldsymbol{g_y}$ and $\boldsymbol{g_u}$ are the system Jacobian matrices; $\Delta\boldsymbol{x} = \boldsymbol{x} - \boldsymbol{x}_0$, $\Delta\boldsymbol{y} = \boldsymbol{y} - \boldsymbol{y}_0$, $\Delta\boldsymbol{u} = \boldsymbol{u} - \boldsymbol{u}_0$; and $\boldsymbol{w}$ are output measurements.

B. Modal Analysis

The eigenvalues and the associated right and left eigenvectors of the open-loop power system $\Delta\dot{\boldsymbol{x}} = \boldsymbol{A}\Delta\boldsymbol{x}$ can be obtained by solving a conventional eigenvalue problem. The geometric observability/controllability are defined as follows [15]. The geometric observability $gm_{o\mu}(k)$ of the mode λ_k from output $\boldsymbol{w}_\mu$ is:

$$gm_{o\mu}(k) = \cos(\theta_1(\boldsymbol{c}_\mu^T, \boldsymbol{\phi}_k)) = \frac{|\boldsymbol{c}_\mu\boldsymbol{\phi}_k|}{||\boldsymbol{\phi}_k||\ ||\boldsymbol{c}_\mu||} \ , \tag{3}$$

where $\boldsymbol{c}_\mu$ is the μ_{th} row of the output matrix $\boldsymbol{C}$; θ_1 is the acute angle between $\boldsymbol{c}_\mu$ and the right eigenvector $\boldsymbol{\phi}_k$; $|\cdot|$ and $||\cdot||$ are the modulus and Euclidian norm, respectively. The geometric controllability $gm_{c\nu}(k)$ of the mode λ_k from input $\boldsymbol{u}_\nu$ is:

$$gm_{c\nu}(k) = \cos(\theta_2(\boldsymbol{\psi}_k, \boldsymbol{b}_\nu)) = \frac{|\boldsymbol{b}_\nu\boldsymbol{\psi}_k|}{||\boldsymbol{\psi}_k||\ ||\boldsymbol{b}_\nu||} \ , \tag{4}$$

where $\boldsymbol{b}_\nu$ is the ν_{th} column of the input matrix $\boldsymbol{B}$; θ_2 is the acute angle between $\boldsymbol{b}_\nu$ and the left eigenvector $\boldsymbol{\psi}_k$.

Based on these measures, a comparison among different outputs and inputs can be carried out, so that the ones that provide the maximum joint geometric observability/controllability measure are selected. The joint observability/controllability measure is defined by:

$$gm_{cok}(\mu, \nu) = gm_{c\nu}(k)\ gm_{o\mu}(k) \ . \tag{5}$$

C. Wide-Area Power System Stabilizer (WAPSS)

The WAPSS in this study is a decentralized controller installed at the j_{th} synchronous machine. The wide area stabilizing signal v_{si} is a differential frequency of the form:

$$v_{si} = \omega_{\text{rem}} - \omega_{\text{G}j} \ , \tag{6}$$

where $\omega_{\text{G}j}$ is the local rotor speed of the j_{th} synchronous machine; ω_{rem} is the remote signal. The remote signal may be a rotor speed ($\omega_{\text{G}i}$), a bus frequency ($\omega_{\text{B}i}$), or the COI frequency of a remote area ($\omega_{\text{coi},i}$). The COI angular frequency of the area i is defined by the following algebraic equation:

$$\omega_{\text{coi},i} = \sum_{j=1}^{q} \frac{H_j}{H_T}\omega_{\text{G}j} \tag{7}$$

where H_j is the inertia of the j_{th} machine of the area i with $j \leq q$ and $H_T = \sum_{j=1}^{q} H_j$.

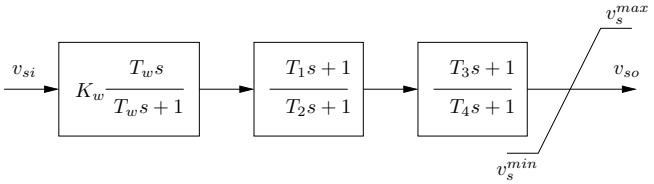

Fig. 1: WAPSS block diagram.

In Fig. 1, K_w is the WAPSS gain, T_w is the washout time constant, T_1, T_2, T_3, T_4 are the four stabilizing blocks time constants, v_1, v_2, v_3 are the WAPSS state variables and v_{so} the output signal. The output signal v_{so} is an additional input to the local Automatic Voltage Regulator (AVR) initial reference (v_0^{ref}), so that the controller damps electromechanical oscillations through excitation control.

D. Time Delays

Introducing time delays in power systems changes the set of DAEs (1) into a set of DDAEs as follows [16]:

$$\begin{aligned} \dot{\hat{\boldsymbol{x}}} &= \hat{\boldsymbol{f}}(\hat{\boldsymbol{x}}, \hat{\boldsymbol{y}}, \hat{\boldsymbol{x}}_d, \hat{\boldsymbol{y}}_d) \\ \boldsymbol{0} &= \hat{\boldsymbol{g}}(\hat{\boldsymbol{x}}, \hat{\boldsymbol{y}}, \hat{\boldsymbol{x}}_d) \ , \end{aligned} \tag{11}$$

where $\hat{\boldsymbol{x}}_d$ and $\hat{\boldsymbol{y}}_d$ are the delayed state and algebraic variables, respectively. In this study, the delays are included in the remote signals. The delayed control signal is:

$$\omega_{\text{rem,d}} = \omega_{\text{rem}}(t - \tau(t)). \tag{12}$$

where the delay $\tau(t)$ is of the form:

$$\tau(t) = \tau_0 + \tau_p(t) + \tau_s(t) \ , \tag{13}$$

where τ_0, $\tau_p(t)$ and $\tau_s(t)$ are the constant, the periodic and the stochastic component of the delay, respectively [7]. The profile of the delay model utilized is shown in Fig. 2.

III. Frequency Estimations

The FDF is a general expression which was proposed in [12] for the estimation of the frequency at the buses of a transmission system. In per units, the FDF reads:

$$\Delta\boldsymbol{\omega}_{\text{B}} = \boldsymbol{D}\Delta\boldsymbol{\omega}_{\text{G}} \ , \tag{14}$$

where $\Delta\boldsymbol{\omega}_{\text{B}}$ and $\Delta\boldsymbol{\omega}_{\text{G}}$ are the deviations of bus frequencies and the synchronous machines rotor speeds, respectively, with respect to the reference frequency; and $\boldsymbol{D}$ is the FDF matrix that is obtained based on network susceptance matrices.

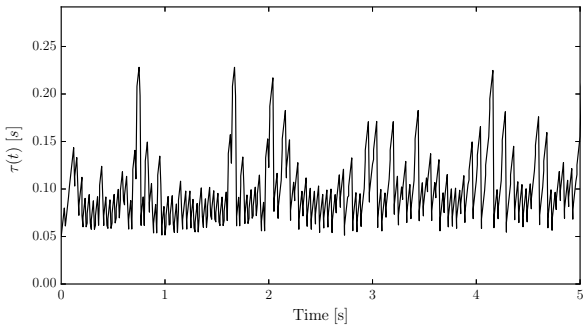

Fig. 2: Time delay profile.

The inverse of the FDF can be utilized to estimate the rotor speeds of synchronous machines from bus frequency measurements provided by PLLs, as follows:

$$\Delta\boldsymbol{\omega}^{*}_{\mathrm{G}} = \boldsymbol{D}^{+}\Delta\tilde{\boldsymbol{\omega}}_{\mathrm{B}} \ , \tag{15}$$

where $\Delta\tilde{\boldsymbol{\omega}}_{\mathrm{B}}$ are the bus frequency deviations obtained from the PLLs; $\Delta\boldsymbol{\omega}^{*}_{\mathrm{G}}$ are the estimated rotor speeds; and $\boldsymbol{D}^{+}$ is the Moore-Penrose pseudo inverse of $\boldsymbol{D}$. A relevant property of $\boldsymbol{D}^{+}$ is that is very sparse. This allows estimating each rotor speed with a small number of bus frequency measures (e.g., two for generator connected in antenna to the grid). All properties of $\boldsymbol{D}^{+}$ are given in [13].

The signals $\Delta\tilde{\boldsymbol{\omega}}_{\mathrm{B}}$ are obtained through a PLL, as follows. The three-phase voltage (v_{abc}) at the connection bus is input to the Phase Detector (PD), which computes the q-axis component v_q. The Loop Filter (LF) inputs the error between v_q and the estimated $\tilde{v}_q$ and outputs the estimated frequency deviation $\Delta\tilde{\omega}_{\mathrm{B}i}$ at bus i. The basic scheme of a PLL is shown in Fig. 3.

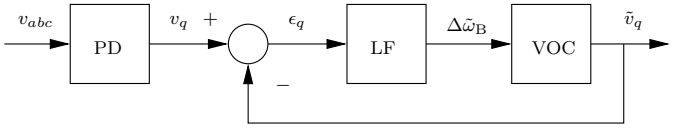

Fig. 3: PLL block diagram.

The dynamic performance of the PLL depends on the implementation of the LF. The case study below compares three PLL configurations that can provide accurate estimations, namely Lag-PLL, Low-Pass Filter PLL (LPF-PLL) and Synchronous Reference Frame PLL (SRF-PLL) [17].

IV. Case Study

The system considered in this study is shown in Fig. 4 [1]. It consists of two identical areas connected through a relatively weak tie; eleven buses $\mathrm{B1}, \mathrm{B2}, ..., \mathrm{B11}$ and four synchronous machines $\mathrm{G1}, \mathrm{G2}, \mathrm{G3}, \mathrm{G4}$ connected at the medium voltage level of 20 kV; the nominal voltage of the transmission system is 230 kV. Each machine is equipped with an AVR of type IEEE DC-1 and a turbine governor. In order to obtain estimations of the wide area signals in a more realistic way, noise is added to the load connected at B7.

All results discussed in this section are obtained with Dome, a Python-based software tool for power system analysis [18].

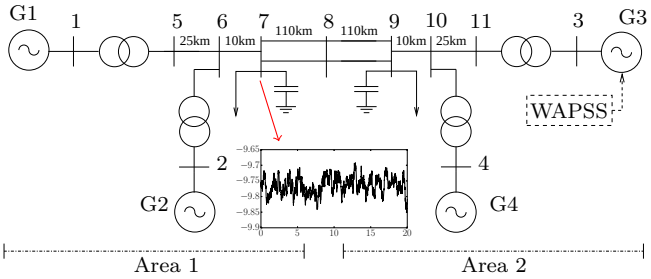

Fig. 4: Two-area four-machine test system.

A. Scenarios

Three scenarios regarding the availability of remote signal measurements are examined, as follows.

- *SC1*: rotor speed signals, ideal bus frequencies and the area-1 COI frequency are assumed to be available. This is the scenario commonly considered in literature. Equation (14) provides the ideal bus frequencies (free of measurement noise and latency).
- *SC2*: rotor speeds are not directly available but all bus frequencies are measurable. Realistic bus frequency measurements are obtained with PLLs. Rotor speeds and area-1 COI frequency are estimated with (15).
- *SC3*: rotor speeds are not available and generators terminal bus frequencies are not measurable. The generators terminal buses, the rotor speed signals and the regional COI frequency are all estimated with (15).

The three scenarios are summarized in Table I.

TABLE I: Bus measurements needed for signal estimation.

Scenario	Signal	Symbol	Available	FDF Est.
SC1	Rotor Speed	$\omega_{\mathrm{G}i}$	✓	✗
	Machine bus freq.	$\omega_{\mathrm{B}i}$	Ideal	✗
	Area-1 COI	$\omega_{\mathrm{COI},1}$	✓	✗
	Other bus freq.	$\omega_{\mathrm{B}i}$	Ideal	✗
SC2	Rotor Speed	$\tilde{\omega}_{\mathrm{G}i}$	✗	✓
	Machine bus freq.	$\tilde{\omega}_{\mathrm{B}i}$	PLL	✗
	Area-1 COI	$\tilde{\omega}_{\mathrm{COI},1}$	✗	✓
	Other bus freq.	$\tilde{\omega}_{\mathrm{B}i}$	PLL	✗
SC3	Rotor Speed	$\hat{\omega}_{\mathrm{G}i}$	✗	✓
	Machine bus freq.	$\hat{\omega}_{\mathrm{B}i}$	✗	✓
	Area-1 COI	$\hat{\omega}_{\mathrm{COI},1}$	✗	✓
	Other bus freq.	$\hat{\omega}_{\mathrm{B}i}$	PLL	✗

B. Open-Loop System (without WAPSS)

The system has a poorly damped inter-area mode $\lambda = -0.102 \pm j3.824$ with natural frequency $f_n = 0.61$ Hz and damping ratio $\zeta = 2.67$ %. Table II shows that the input placement with the highest controllability of λ is the AVR of G3. In the remainder of the case study, we focus on the following wide area signals according to the discussion in Section II: differential rotor speed G1-G3, differential frequency B1-G3, and differential frequency COI 1-G3.

The geometric measures of the local signal ω_{G3} as well as of the wide area signals for *SC1* are shown in Table

TABLE II: Controllability of λ from j-th AVR.

j	1	2	3	4
gm_c	$1.94 \cdot 10^{-5}$	$1.67 \cdot 10^{-5}$	$3.06 \cdot 10^{-5}$	$2.46 \cdot 10^{-5}$

TABLE III: Geometric measures of λ from wide area signals.

Signal	gm_o	gm_{co}
ω_{G3}	$1.95 \cdot 10^{-3}$	$5.98 \cdot 10^{-8}$
$\omega_{\mathrm{G1}} - \omega_{\mathrm{G3}}$	$2.59 \cdot 10^{-3}$	$7.93 \cdot 10^{-8}$
$\omega_{\mathrm{B1}} - \omega_{\mathrm{G3}}$	$2.75 \cdot 10^{-3}$	$8.42 \cdot 10^{-8}$
$\omega_{\mathrm{COI},1} - \omega_{\mathrm{G3}}$	$2.88 \cdot 10^{-3}$	$8.82 \cdot 10^{-8}$

III. As expected, wide area signals have better observability/controllability than local rotor speeds.

The bus measurements required by the FDF to estimate the examined remote signals in *SC2* and *SC3* are summarized in Table IV.

TABLE IV: Bus measurements utilized by the FDF.

Scenario	Signal	Meas. 1	Meas. 2	Meas. 3	Meas. 4
SC2	$\tilde{\omega}_{\mathrm{G1}}$	B1	B5	–	–
SC2	$\tilde{\omega}_{\mathrm{coi},1}$	B1	B2	B5	B6
SC3	$\hat{\omega}_{\mathrm{G1}}$	B5	B6	–	–
SC3	$\hat{\omega}_{\mathrm{B1}}$	B5	B6	–	–
SC3	$\hat{\omega}_{\mathrm{coi},1}$	B5	B6	B7	–

The remainder of this section considers the transient following the tripping of one of the transmission lines that connects B7 with B8. The contingency occurs at $t = 0.2$ s and normal operation is restored after 1 s.

Comparative results on the estimated rotor speed $\tilde{\omega}_{\mathrm{G1}}$ (see *SC2*) are plotted in Fig. 5. The average errors of the FD estimations for scenarios *SC2* and *SC3* are summarized in Table V. The average errors of the FD estimations are in the order of 10^{-5} for both *SC2* and *SC3* and for all three PLLs.

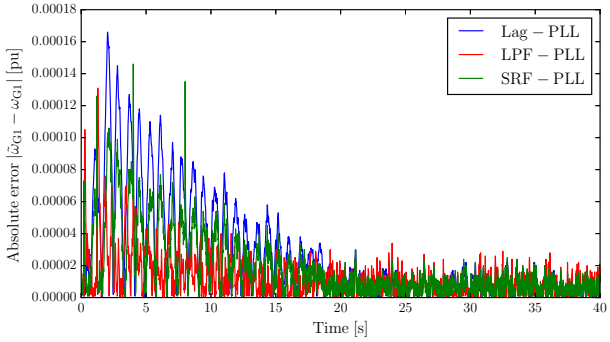

Fig. 5: Absolute error $|\tilde{\omega}_{\mathrm{G1}} - \omega_{\mathrm{G1}}|$.

TABLE V: Mean absolute errors of FD estimations.

Error	Lag-PLL	LPF-PLL	SRF-PLL
$\tilde{\omega}_{\mathrm{G1}} - \omega_{\mathrm{G1}}$	$2.62 \cdot 10^{-5}$	$1.30 \cdot 10^{-5}$	$1.76 \cdot 10^{-5}$
$\tilde{\omega}_{\mathrm{coi},1} - \omega_{\mathrm{coi},1}$	$2.35 \cdot 10^{-5}$	$1.39 \cdot 10^{-5}$	$1.26 \cdot 10^{-5}$
$\hat{\omega}_{\mathrm{G1}} - \omega_{\mathrm{G1}}$	$2.66 \cdot 10^{-5}$	$1.55 \cdot 10^{-5}$	$1.88 \cdot 10^{-5}$
$\hat{\omega}_{\mathrm{B1}} - \omega_{\mathrm{B1}}$	$2.30 \cdot 10^{-5}$	$1.22 \cdot 10^{-5}$	$1.64 \cdot 10^{-5}$
$\hat{\omega}_{\mathrm{coi},1} - \omega_{\mathrm{coi},1}$	$2.43 \cdot 10^{-5}$	$1.81 \cdot 10^{-5}$	$1.54 \cdot 10^{-5}$

A comparison between the ideal and LPF-PLL based bus frequency measurements is shown in Figs. 6–7. The stochasticity of the load connected at B7 has a significant impact on the estimation of the bus frequencies by the PLL. However, this does not deteriorate the estimations based on the FDF, as shown in Table V. The FDF estimated remote signals for *SC3* are shown in Fig. 8.

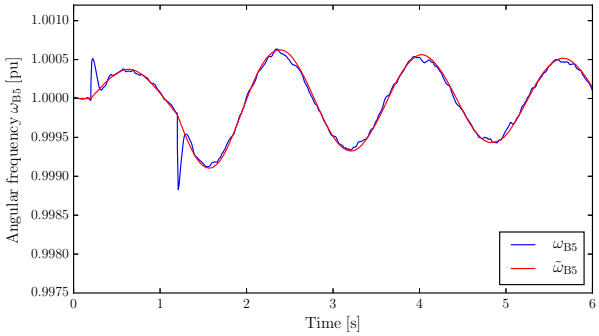

Fig. 6: Frequency measurement at bus B5.

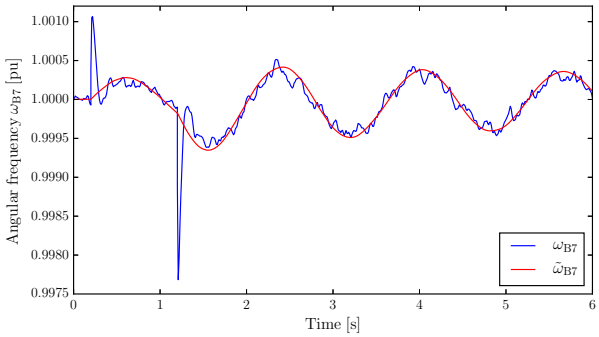

Fig. 7: Frequency measurement at bus B7.

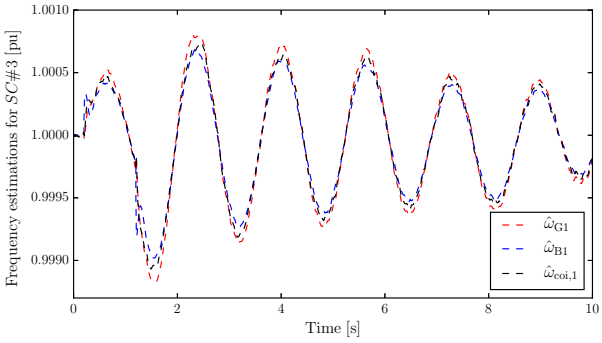

Fig. 8: FDF estimations for *SC3*.

C. Closed-Loop System (with WAPSS)

The WAPSS is connected to the AVR of G3. Figure 9 shows the G2 rotor speed transient response for different wide area signals. The open loop system response is also shown for reference. The wide area signals effectively damp the inter-area mode. The three examined signals provide similar

overshoot and settling time. This is expected as the frequency at a machine terminal bus response is strongly dependent on the rotor speed of the machine itself. Moreover, the area-1 COI for the two-area system consists of two machines with the same inertia and thus, its associated dynamics does not differ significantly from that of each rotor speed.

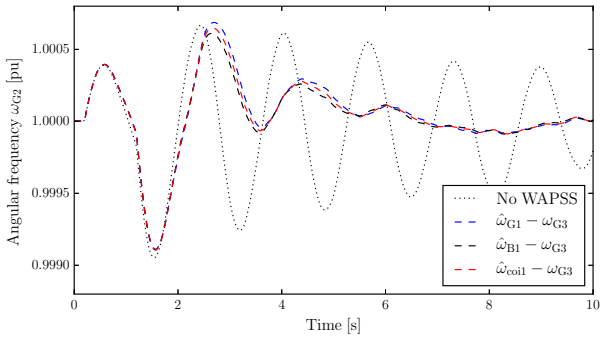

Fig. 9: G2 rotor speed with different wide area signals.

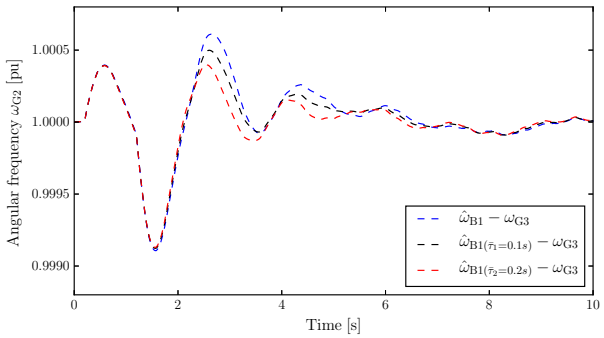

Fig. 10: G2 rotor speed with delayed remote signal.

Next, the quasi-periodic stochastic delays described in Subection II-D are included in the wide area signals. Two delays $\tau_1(t)$ and $\tau_2(t)$ are examined, with mean values 100 ms and 200 ms, respectively. The rotor speed of G2 when the WAPSS utilizes the differential frequency B1-G3 is shown in Fig. 10.

Even though the delays are mostly known to impact negatively on the stability of power systems, this is not the case of the trajectories shown in Fig. 10. The system performance actually improves with the inclusion of the delays.

V. Conclusions

The paper discusses a WAPSS for damping inter-area oscillations. The focus is on the utilization of realistic bus frequency measurements and the FDF to obtain wide area signals. A comparison among different PLL models for frequency estimation on the two-area system serves to illustrate the accuracy of the FDF estimations.

Simulation results show that the utilization of the remote area information is enough to damp the inter-area mode. In order to examine the effectiviness of COI-based wide area signals, a test system with more synchronous machines per area and different machine parameters is required.

An interesting result of this paper is that the inclusion of communication delays has a positive impact on the overall system performance. The change of the dominant local modes with respect to the controller gain and the applied delay has only recently been studied using stability maps [19]. Such stability maps can also be used to understand the stability properties of a system with a WAPSS employed to damp inter-area oscillations. Future work will move towards this direction.

References

[1] P. Kundur, *Power system stability and control*. New York: Mc-Grall Hill, 1994.

[2] J. H. Chow, J. J. Sanchez-Gasca, H. Ren, and S. Wang, "Power system damping controller design-using multiple input signals," *IEEE Control Systems Magazine*, vol. 20, no. 4, pp. 82–90, Aug. 2000.

[3] I. Kamwa, R. Grondin, and Y. Hebert, "Wide-area measurement based stabilizing control of large power systems-a decentralized/hierarchical approach," *IEEE Trans. on Power Systems*, vol. 16, no. 1, pp. 136–153, Feb. 2001.

[4] M. E. Aboul-Ela, A. A. Sallam, J. D. McCalley, and A. A. Fouad, "Damping controller design for power system oscillations using global signals," *IEEE Trans. on Power Systems*, vol. 11, no. 2, pp. 767–773, May 1996.

[5] H. Wu, K. S. Tsakalis, and G. T. Heydt, "Evaluation of time delay effects to wide-area power system stabilizer design," *IEEE Trans. on Power Systems*, vol. 19, no. 4, pp. 1935–1941, Nov. 2004.

[6] S. Wang, X. Meng, and T. Chen, "Wide-area control of power systems through delayed network communication," *IEEE Trans. on Control Systems Technology*, vol. 20, no. 2, pp. 495–503, Mar. 2012.

[7] M. Liu, I. Dassios, G. Tzounas, and F. Milano, "Stability analysis of power systems with inclusion of realistic-modeling of WAMS delays," *IEEE Trans. on Power Systems*, pp. 1–1, 2018.

[8] A. Heniche and I. Kamwa, "Assessment of two methods to select wide-area signals for power system damping control," *IEEE Trans. on Power Systems*, vol. 23, no. 2, pp. 572–581, May 2008.

[9] Y. Wang, P. Yemula, and A. Bose, "Decentralized communication and control systems for power system operation," *IEEE Trans. on Smart Grid*, vol. 6, no. 2, pp. 885–893, Mar. 2015.

[10] J. W. Stahlhut, T. J. Browne, G. T. Heydt, and V. Vittal, "Latency viewed as a stochastic process and its impact on wide area power system control signals," *IEEE Trans. on Power Systems*, vol. 23, no. 1, pp. 84–91, Feb. 2008.

[11] R. Hadidi and B. Jeyasurya, "Reinforcement learning based real-time wide-area stabilizing control agents to enhance power system stability," *IEEE Trans. on Smart Grid*, vol. 4, no. 1, pp. 489–497, Mar. 2013.

[12] F. Milano and Á. Ortega, "Frequency divider," *IEEE Trans. on Power Systems*, vol. 32, no. 2, pp. 1493–1501, Mar. 2017.

[13] F. Milano, Á. Ortega, and A. J. Conejo, "Model-agnostic linear estimation of generator rotor speeds based on phasor measurement units," *IEEE Trans. on Power Systems*, vol. 33, no. 6, pp. 7258–7268, Nov. 2018.

[14] F. Milano, "Rotor speed-free estimation of the frequency of the center of inertia," *IEEE Trans. on Power Systems*, vol. 33, no. 1, pp. 1153–1155, Jan. 2018.

[15] H. Hamdan and A. Hamdan, "On the coupling measures between modes and state variables and subsynchronous resonance," *Electric Power Systems Research*, vol. 13, no. 3, pp. 165 – 171, 1987.

[16] F. Milano and M. Anghel, "Impact of time delays on power system stability," *IEEE Trans. on Circuits and Systems - I: Regular Papers*, vol. 59, no. 4, pp. 889–900, Apr. 2012.

[17] Á. Ortega and F. Milano, "Comparison of different PLL implementations for frequency estimation and control," in *Procs. of the 18th International Conference on Harmonics and Quality of Power (ICHQP)*, May 2018, pp. 1–6.

[18] F. Milano, "A Python-based software tool for power system analysis," in *Procs. of the IEEE PES General Meeting*, Vancouver, BC, Jul. 2013.

[19] V. Bokharaie, R. Sipahi, and F. Milano, "Small-signal stability analysis of delayed power system stabilizers," in *2014 Power Systems Computation Conference*, Aug. 2014, pp. 1–7.